Spectroscopy of Mn^{4+}-doped Ca-substituted gadolinium gallium garnet

A. Brenier, Andrzej Suchocki,* C. Pedrini, G. Boulon, and C. Madej
Laboratoire de Physico-Chimie des Matériaux Luminescents, Université Claude Bernard Lyon I, Bâtiment 205, 43, boulevard du 11 Novembre 1918, 69622 Villeurbanne CEDEX, France
(Received 26 December 1991)

The results of optical studies of Ca- and Mg-substituted $Gd_3Ga_5O_{12}$ garnets doped with Mn^{4+} are reported. Multiple sites of Mn^{4+} ions are revealed at liquid-helium temperature by laser excitation and emission spectra and analysis of decay kinetics. Use of different charge-compensating ions allows one to obtain information on the nature of some sites occupied by the Mn^{4+} ions. A large Stokes shift between excitation and luminescence spectra of the ^2E state of Mn^{4+} ions is explained by interaction with low-energy lattice excitations. On the other hand, the higher-energy phonons are found to be responsible for nonradiative decay of the Mn^{4+} luminescence at higher temperatures. Charge-transfer states are present in the crystals examined.

I. INTRODUCTION

The Mn^{4+} ion has the same electronic structure of the last open shell as $Cr^{3+}(d^3)$. both ions are known to occupy several various sites in the garnet host, giving rise to rather complicated optical spectra. Multiple-site properties of Cr^{3+} ions in garnets has been studied in our laboratory in the past. The Mn^{4+} ion can be a very promising system for tunable laser application, as well as Cr^{3+}, either as an active lasing center or as a luminescence coactivator for rare-earth ions.

Though several studies of Mn^{4+} have been performed,[1-5] the detailed nature of the optical properties of this ion still remains vague. The strength of electron-phonon interaction in this ion is an example of such open problems. It has been found that the Mn^{4+} ion interacts with a host much stronger than the similar Cr^{3+} (Ref. 4). This problem shall be addressed in the paper in the framework of the Struck-Fonger single-configurational-coordinate model.[6] The exact nature of observed multiple sites is also very often unknown. We shall present some evidences that charge compensation necessary to obtain manganese ions in the 4+ state induces multiple-site structure of this dopant in the gadolinium gallium garnet (GGG) host.

II. CRYSTAL GROWTH AND EXPERIMENTAL SETUPS

The crystals have been grown by the Czochralski technique under a gas flow of nitrogen (480 l/h) and oxygen (4.8 l/h) in order to decrease gallium oxide decomposition. The pull rate was 0.4 cm/h and the rotation rate varied according to the crystal length from 6 to 15 rpm. The crystal size was 3 cm diameter and 10 cm length. The crystal was pulled along the ⟨111⟩ axis. Manganese was added in the form of MnO_2. An equal quantity of charge-compensating Ca^{2+} ions was added to the melt in the form of $CaCO_3$. The starting composition of the melt was

$$\{Gd_{3-x}Ca_x\}|Ga_{1.95-x}Mn_xGd_{0.5}|(Ga_3)O_{12}$$

with $x=4.95\times10^{-3}$. The symbols { }, | |, and ( ) stand, respectively, for dodecahedral, octahedral, and tetrahedral sites. The segregation coefficient of the Mn ions is less than unity giving an increase in the red color of the crystals along its axis.

The absorption spectra were recorded with a Cary 2300 spectrophotometer. The luminescence spectra, excited by the 514.5-nm argon-ion laser line or by the 532-nm line of a frequency-doubled pulsed YAG:Nd Quantel laser, have been measured with a Jobin-Yvon HRS1 monochromator equipped with an RCA 31034 cooled photomultiplier (GaAs photocathode) and a PAR model 186A lockin amplifier in the case of the continuous excitation. The luminescence excitation spectra were obtained with a 450-W xenon lamp and a Jobin Yvon H10D monochromator. The laser excitation spectra and the emission spectra from selective excitations were obtained with the use of a Lumonics dye laser with LD 690 dye pumped by a XeCl Lumonics excimer laser. The resolution of the dye laser was equal to 0.1 cm^{-1}. The luminescence decay kinetics of the Mn luminescence were excited at 532 nm and were stored in a model 9400A Lecroy digital oscilloscope and analyzed by a computer. The samples were placed in various cryostats to perform temperature measurements. The two-photon time-resolved laser excitation spectra were obtained with a 532-nm pumped dye laser and a Raman shifter hydrogen cell. The infrared beam of energy of 1 mJ was focused a few cm before the sample and was carefully cleaned of any red light by using a proper set of filters. The Raman spectra were recorded at room temperature in a DILOR 5-grating Raman spectrophotometer.

III. EXPERIMENTAL RESULTS

A. Absorption, luminescence, and photoluminescence excitation spectra

The temperature dependence of luminescence spectra, excited by the 514.5-nm Ar^+ laser line, of the

GGG:Mn^{4+} crystal in the region of 590–750 nm is shown in Fig. 1. The spectra consist of two, relatively sharp (at low temperatures) lines at 663.5 and 668 nm and a broader structure, peaked at 681 nm. At higher temperatures these lines are considerably broadened and they are not resolved at 200 K and above. They are related to two different sites for manganese ions, which we call "A" and "B," respectively, and they are consistent with luminescence of $Mn^{4+}(d^3)$ ions in relatively strong crystal field with the ^2E state being the first excited state. These sites have different luminescence excitation spectra. The broader structure at 681 nm is due to vibronic transitions, which will be shown later.

The absorption and the photoluminescence excitation (PLE) spectra of sharp lines in the region of Mn^{4+} intrashell transitions (400–600 nm) at $T=10$ K are shown in Fig. 2. The luminescence was excited here by a xenon lamp with a relatively low resolution. The absorption band, peaked at around 500 nm, is due to transitions from the ground $^4A_2$ state to the first excited quartet state, $^4T_2$. The band is a convolution of transitions of various sites. The excitation spectra of 663.5- and 668-nm lines are different. No transitions to the doublet excited states are visible in the absorption neither in these PLE spectra.

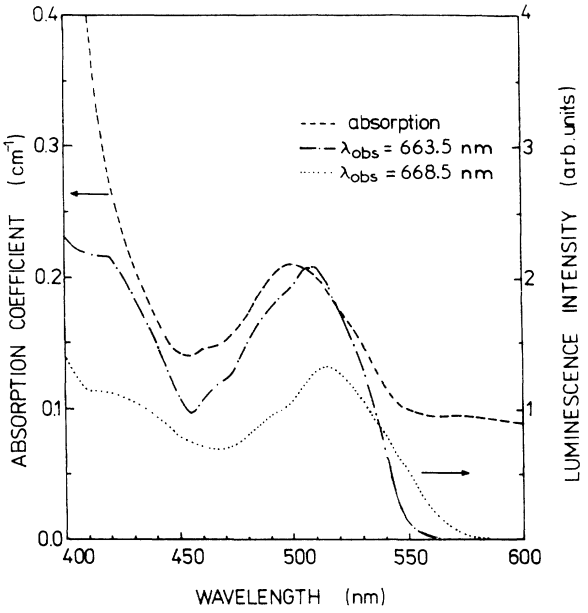

FIG. 2. The absorption and luminescence excitation spectra of the GGG:Mn^{4+} sample in the region of the intrashell transitions at $T=10$ K.

B. Thin sample spectra

Very strong bands are observed in the absorption and PLE spectra of thin GGG:Mn^{4+} samples in the ultraviolet region (see Fig. 3). They are much stronger than the bands associated with the internal Mn^{4+} transitions. These bands occur at the same spectral position in both absorption and PLE spectra. The intensities of the bands in the PLE measurements diminish when temperature is raised, although the deactivation energies depend on dopant concentration. These bands are due to charge-transfer transitions. Similar spectra have also been observed for GGG:V^{4+} crystals.[7] The sharp line at 270 nm is due to Gd^{3+} absorption. The transitions to the higher excited quartet states, $^4T_1$, can be seen in the PLE and

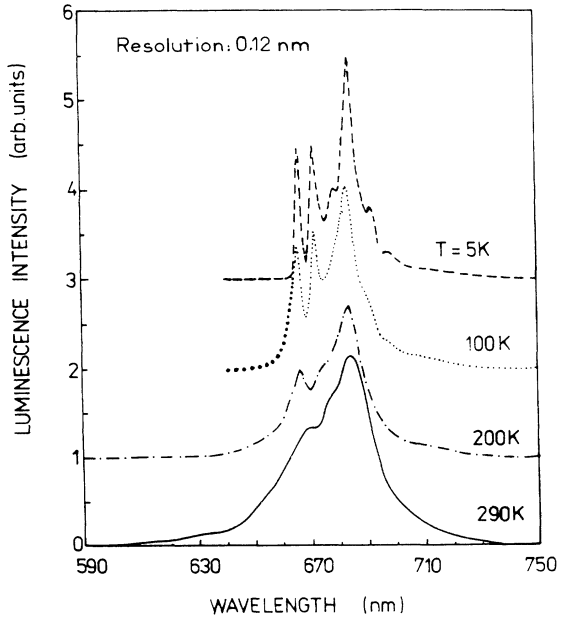

FIG. 1. Temperature dependence of the luminescence spectra of the GGG:Mn^{4+} crystal, excited by a 514.5-nm argon-ion laser line.

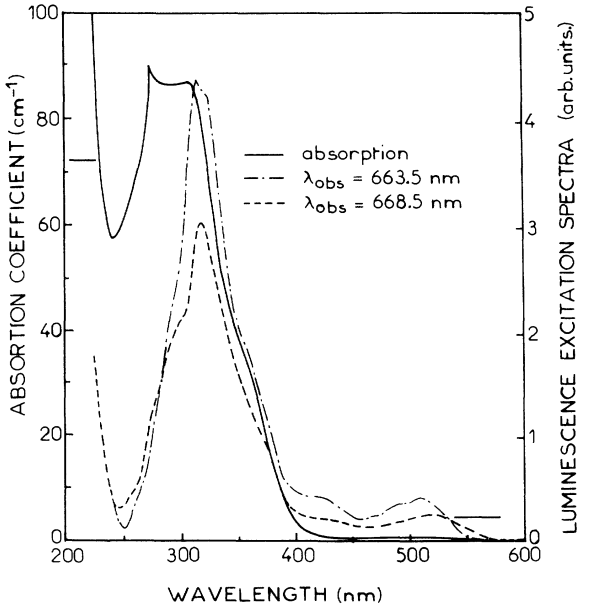

FIG. 3. Absorption and PLE spectra of the thin GGG:Mn^{4+} crystal in the region of charge-transfer transitions.

absorption spectra around 370 nm on the shoulder of the charge-transfer band. The exact spectral position of the $^4T_1$ state is difficult to establish due to large overlap with much stronger charge-transfer transitions.

C. Time-resolved spectra

The time-resolved luminescence spectra, taken at $T=10$ K, presented in Fig. 4, confirmed that the 663.5- and 668-nm lines are due to different sites. The spectra, taken at different times after the excitation pulse of the laser, show that the line assigned to center B has a much shorter lifetime than the line from center A. It can also be seen that the broader structure, peaked at 681 nm, is mostly associated with the A manganese center.

D. Laser spectroscopy

In order to obtain the PLE spectra of the Mn^{4+} sharp transitions with high resolution, the laser excitation has been applied. Liquid-helium-temperature laser excitation spectra of 663.5- and 668-nm emissions can be seen in Fig. 5(a). Each of them has two peaks which are rather broad: about 60 cm^{-1} (FWHM). The maximum of the main peak is at 660.5 nm for the spectrum which is labeled A and at 667 nm for the B one. By selective laser excitation at these two wavelengths, we obtained the two A and B emission spectra, presented in Fig. 5(b). The A spectrum has a sharp line and a broad structure peaking at 663.8 and 681 nm, respectively. The B spectrum has mainly a sharp line peaking at 668 nm and a weak structure visible up to 700 nm. The laser excitation spectrum of the 681-nm emission is the sum of the A and B spectra of Fig. 5(a), the A spectrum being dominant. By recording laser excitation spectra at different emission wavelengths, we had found that the 671-nm emission had a different excitation spectrum than the A and B ones (see Fig. 6, curve b). By selective laser excitation at the maximum of the lines of this new spectrum (670 nm), we have obtained a third emission spectrum (Fig. 6, curve a) peaking at 671 nm and also having a weak broad structure up to 700 nm. The most striking feature that can be observed in these spectra is the very large spectral shift between the laser PLE and emission spectra of each center,

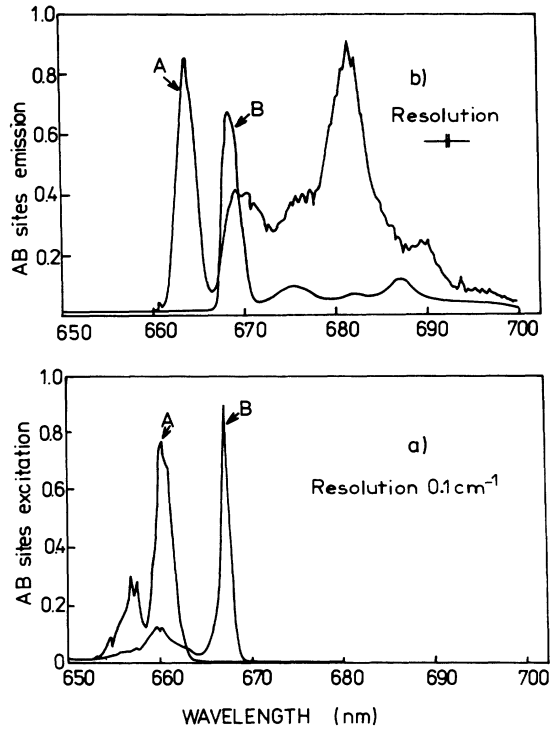

FIG. 5. (a) Laser excitation spectra of 663.5- and 668-nm emissions. (b) Emission spectra excited at 660.5 nm, curve A, and at 667 nm, curve B. Spectra are taken at $T=8$ K.

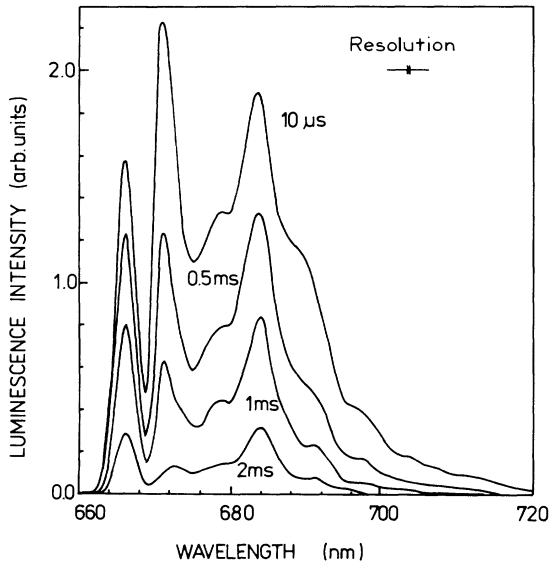

FIG. 4. Time-resolved luminescence spectra of the GGG:Mn^{4+} crystal, taken at $T=10$ K. The delay times are shown in the graph.

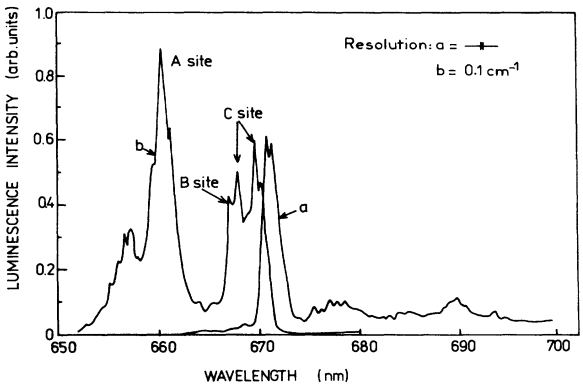

FIG. 6. Emission spectrum excited at 670 nm (curve a) and laser excitation spectrum of 671-nm emission (curve b). Spectra are taken at $T=8$ K.

equal to approximately 68, 23, and 22 cm^{-1} for the *A*, *B*, and *C* centers, respectively. (We have checked that the mismatching between the dye laser and the monochromator calibrations was less than 0.5 cm^{-1}.)

E. Decay kinetics

The decay kinetics of manganese luminescence excited in the $^4T_2$ band, measured at the peak of center *A* luminescence (i.e., $\lambda_A = 663.5$ nm), are single exponential at low temperatures with the decay time equal to (1280±90) μs at $T = 10$ K. The decay kinetics, taken at the peak of center *B* luminescence (i.e., $\lambda_B = 668$ nm) exhibits double-exponential behavior at low temperatures, with the longer decay time equal to the decay time of center *A* and a decay time of the shorter component equal to (445±40) μs at low temperatures. The kinetics, measured at the peak of center *C* luminescence (i.e., $\lambda_B = 671$ nm), and measured under selective excitation of center *C*, is again single exponential with the decay time equal to (370±10) μs at $T = 10$ K. Decay kinetics of the *A* and *B* centers excited selectively are also single exponential at low temperatures. At higher temperatures the decay kinetics usually exhibit several-exponential behavior due to large overlap of the various centers luminescence spectra. The temperature dependence of the luminescence decay times of centers *A* and *B* are presented in Fig. 7. The decay time of center *C* is also shown in this figure for $T = 10$ K only, since a large overlap between center *C* and center *B* luminescences, which have similar decay times, does not allow one to obtain clear results at higher temperatures.

F. Time-resolved two-photon laser excitation spectra

Two-photon transitions very often have different selection rules than one-photon ones. Therefore, two- and one-photon spectra can be viewed as complementary in such a sense like Raman and far-infrared spectra. It is also a case of electric dipole transition between the $^2E \leftrightarrow {}^4A_2$ states in octahedral symmetry, which are forbidden in one-photon and allowed in two-photon spectra.[8] In order to check whether a large shift between PLE and emission of the $^2E \leftrightarrow {}^4A_2$ one-photon transitions is related to their forbidden character, the two-photon spectra have been measured. The spectra were recorded at 10 K. Since the luminescence was weak, the Mn fluorescence has been detected without any spectral selection. Time-resolved spectra provided a method to distinguish the different Mn^{4+} sites. The *A* Mn fluorescence is detected only if the spectra are recorded at longer times (i.e., 1.4 ms) after the excitation pulse since the *B* and *C* Mn fluorescences have lifetimes that are too short (450 and 370 μs, respectively) to be detected. The *A* two-photon spectrum is presented in Fig. 8. It can be superimposed with the one-photon excitation spectrum if the wavelength scale is divided by 2. When the delay is equal to 0.3 ms, the whole Mn fluorescence is detected and in the range of 666–668 nm we obtain the *B* two-photon excitation spectrum peaking at 667 nm (after correction of the wavelength scale) like the one-photon one (see Fig. 9). The two-photon spectra do not reveal any additional structure than the one-photon ones.

G. Influence of various charge compensation

The Ca^{2+} ions in the GGG host are located in the dodecahedral sites and the Mn^{4+} ions in the octahedral ones. Because the shortest distance between these two sites is almost two times smaller than the shortest distance between two octahedral sites, we have checked if the Mn fluorescence is affected by using charge-compensating ions which are located in the octahedral sites. This was done by measuring the fluorescence of a new crystal grown in our laboratory, doped with Mn/(Mg), since Mg^{2+} ions go preferentially into octahe-

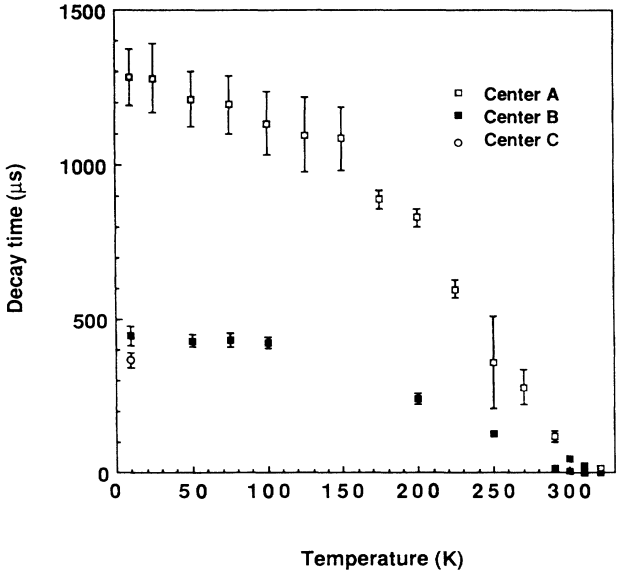

FIG. 7. Temperature dependence of the luminescence decay times of different manganese centers in GGG crystals.

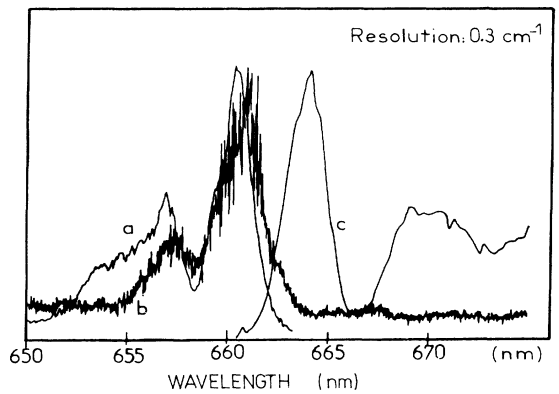

FIG. 8. One- and two-photon excitation and emission spectra of GGG:(Mn^{4+},Ca^{2+}) for center *A* at $T = 10$ K. *a*, one-photon excitation spectra; *b*, two-photon excitation spectra (delay is equal to 1.4 ms); *c*, emission spectra, excited at the peak of the excitation spectra. The wavelength scale for two-photon spectra has been multiplied by 2.

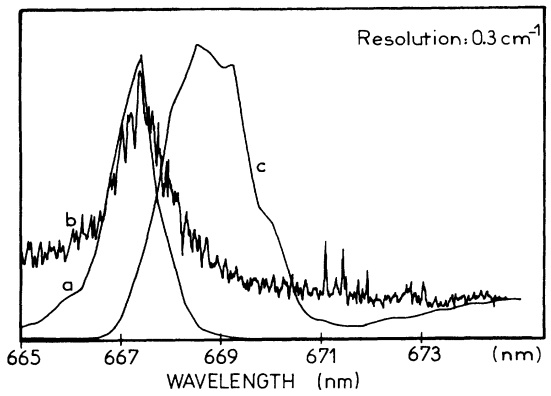

FIG. 9. One- and two-photon excitation and emission spectra of GGG:(Mn^{4+},Ca^{2+}) for center B at $T=10$ K. a, one-photon excitation spectra; b, two-photon excitation spectra (delay is equal to 0.3 ms); c, emission spectra, excited at the peak of the excitation spectra. The wavelength scale for two-photon spectra has been multiplied by 2.

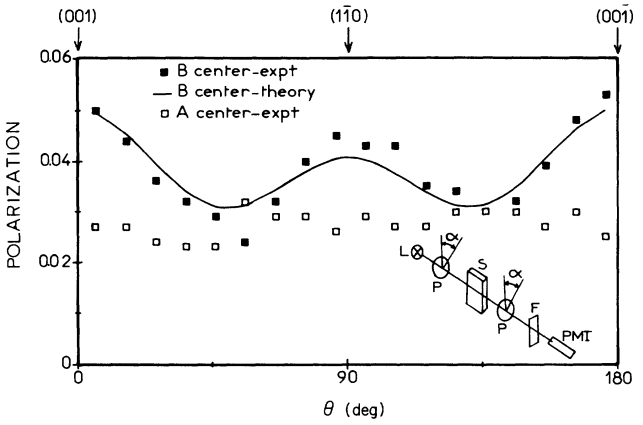

FIG. 11. Azimuthal dependence of the degree of polarization of emission of the A and B centers for a sample cut perpendicular to (110) direction. The experimental arrangement is shown in the right bottom corner: L xenon lamp; P, polarizer; S, sample; F, filter; PMT, photomultiplier.

dral sites in the GGG host.[9] The low-temperature Mn^{4+} fluorescence of the Mg/(Mn) crystal, excited with 500-nm light from a xenon lamp, is compared with the one for the Mn/(Ca) crystal in Fig. 10. The main difference between the two spectra is that the line peaking at 668 nm in the Mn/(Ca) spectrum has almost disappeared in the Mn/(Mg) one. Nevertheless, by a selective laser excitation at 667 nm in the Mn/(Mg) sample, it is possible to record a weak B spectrum which is identical to the one presented in Fig. 5(b) for the Mn/(Ca) crystal.

H. Polarization measurements

Relatively close charge compensation should result in increased probability of electric dipole transitions due to axial distortion of octahedral environment of Mn^{4+} ions.[10] The radiating dipoles should then be oriented along the shortest distances between the Mn^{4+} and Ca^{2+} ions, being nearest neighbors. Such orientation of dipoles induces partial linear polarization of the emission spectra of samples cut along main crystallographic directions, the degree of which depends on the azimuthal position of the examined crystal. The degree of polarization is defined as a ratio:

$$P=\frac{I_{\parallel}-I_{\perp}}{I_{\parallel}+I_{\perp}}\ , \tag{1}$$

where $I_{\parallel}$ and $I_{\perp}$ are emission intensities parallel and perpendicular to the polarization of exciting light, respectively.

The aximuthal dependence of the degree of polarization of emission of the A and B centers (measured at 663.5 and 668 nm at $T=8$ K), excited in the absorption band around 500 nm for a sample cut perpendicular to (110) direction, is shown in Fig. 11. The experimental arrangement of the polarization measurement is shown in the inset in the figure. It can be seen that there is no azimuthal dependence of polarization of light emitted by center A and a weak dependence of center B. The degree of linear polarization of center B is in the range 0.02–0.055. The azimuthal dependence of polarization for samples cut along the (100) axis is more complicated, which may be a result of the greater influence of the dominating magnetic-dipole transitions.

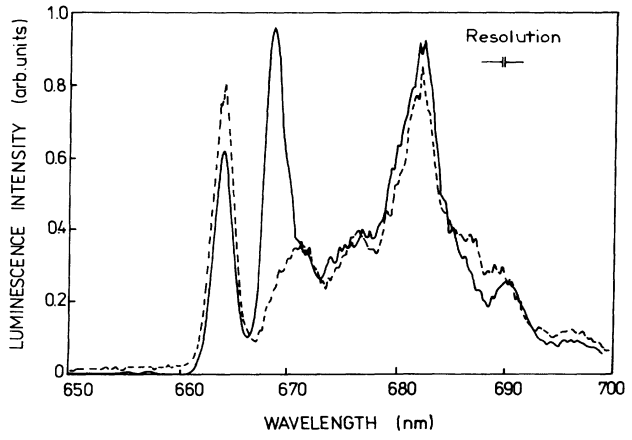

FIG. 10. Emission spectra of GGG:(Mn^{4+},Ca^{2+}) (----) and GGG:(Mn^{4+},Mg^{2+}) (— — —) crystals, excited with 500-nm light from a xenon lamp, measured at $T=5$ K.

IV. DISCUSSION

A. Crystal-field and Racah parameters

The two bands of the excitation spectrum peaking at 370 and 510 nm, the latter one also clearly seen in absorption, are attributed, respectively, to the $^4A_2\rightarrow{}^4T_1$ and $^4A_2\rightarrow{}^4T_2$ transitions of Mn^{4+} ions ($3d^3$) in octahedral coordination. The three emission lines peaking at 663.5, 668, and 671 nm are attributed to the $^2E\rightarrow{}^4A_2$

transition of Mn^{4+} ions and reveal that the octahedra can have three different environments due to the different position of the Ca^{2+} charge-compensating ions as will be explained in the next section. Using the Tanabe-Sugano diagram, the peak of the $^4T_2$ absorption band, and an average value for the position of the zero-phonon ^2E level, we have calculated the crystal field and the Racah parameters:

$$Dq = 1960 \text{ cm}^{-1}, \quad B = 722 \text{ cm}^{-1} .$$

These values can be compared with the ones for Cr^{3+} in GGG and GGG(Ca,Zr):

GGG:Cr: $Dq = 1585 \text{ cm}^{-1}$, $B = 677 \text{ cm}^{-1}$,

GGG(Ca,Zr):Cr: $Dq = 1565 \text{ cm}^{-1}$, $B = 683 \text{ cm}^{-1}$.

The splitting of the ^2E level of each of three sites (i.e., R_1 and R_2 excitation lines) can be observed in the laser excitation spectra (see Figs. 5 and 6). Their values are listed in Table I.

B. Nature of the three Mn^{4+} environments

The 663.5-, 668-, and 671-nm emission lines are attributed to Mn^{4+} ions in different environments which we label *A*, *B*, and *C*, respectively. More precisely, the Mn^{4+} ions are in the octahedral sites of the garnet host and the spin-orbit coupling and the trigonal distortion of the octahedra split the ^2E level into two components: $2A_{3/2}$ and $E_{1/2}$. The last one is the emitting level at liquid-helium temperature and both components are the final levels of the excitation. The smooth lines at 663.5, 668, and 671 nm are zero-optical phonon lines and the broad structures that extend up to 700 nm are due to phonon terminated transitions (phonon sidebands: this is why the spectra seem to be "noisy" in this region). Because the liquid-helium-temperature radiative lifetimes of the *B* and *C* emissions are much shorter than the *A* one, we conclude that the *B* and *C* environments perturb much more strongly the initial octahedral symmetry than the *A* one. We think that in the *B* and *C* cases the Ca^{2+} charge-compensating ions are closer to the Mn ions than in the *A* case. In such a way, the center of inversion is destroyed: the zero-optical phonon $^2E \rightarrow {}^4A_2$ transition becomes electric-dipole-allowed and stronger than its phonon sideband. In the *A* case, the center of inversion is conserved, the zero-phonon transitions are most probably only magnetic-dipole-allowed and weaker than its vibronic sideband. In the Mn-Mg–doped GGG crystal, the smallest Mn-Mg distance is 5.36 Å,[11] and only traces of the *B* and *C* environments are detected. That means that these environments are created by charge-compensating ions which are situated at smaller distances to Mn^{4+} ions than 5.36 Å. The Mn-Ca distance in the Mn-Ca–doped crystal, which only satisfies this condition, is the one between Mn^{4+} and its first Ca^{2+} neighbor, equal to 3.47 Å, and the distance to the second Ca^{2+} neighbor is equal to 5.57 Å. We conclude that, in the Mn-Ca crystal, the *A* environments are due to Ca^{2+} ions situated at least in the position of second neighbors of the Mn^{4+} ions or farther, and the *B* and *C* environments are due to Ca^{2+} ions situated in the position of first neighbor of the Mn^{4+} ions. In the Mn-Mg–doped GGG crystal, the traces of *B* and *C* environments are attributed to a weak occupation of the dodecahedral sites by the Mg^{2+} ions [several garnets with Mg ions in dodecahedral sites are known, for example, $\{Mg_3\}[Al_2](Si_3)O_{12}$].

Azimuthal dependence of the polarization of emission of center *B* and lack of such dependence for center *A* support the above conclusions. In the case of a purely octahedral center, theory predicts no azimuthal dependence of emission, in agreement with experimental data. In order to determine the degree of polarization for Mn^{4+} centers with close charge compensation, it is necessary to take into account the crystallographic structure of GGG and calculate the azimuthal dependence of the relative probability of excitation and emission of the separate groups of dipoles, according to Feofilov theory.[10] Such calculations yield the value of polarization in the order of 0.4–0.6. Since experimental values are of one order smaller, we conclude that the other nonpolarized (or polarized circularly) parts of emission dominate the spectra. This is probably a result of a relatively large separation of Mn^{4+} and Ca^{2+} ions, even if they are first-nearest neighbors. In order to take into account nonpolarized contributions (or polarized circularly) I_n, we fit our data with a modified formula (1), in the form of

$$P = \frac{I_{\parallel} - I_{\perp}}{I_{\parallel} + I_{\perp} + 2I_n} . \tag{2}$$

The solid line in Fig. 11 represents the best fit of formula (2) to the experimental data of the azimuthal dependence of the polarization of center *B*, in very good agreement with observed results.

TABLE I. Wavelengths corresponding to the peak of the $^2E \leftrightarrow {}^4A_2$ transition in laser excitation and emission spectra, the Stokes shifts, ^2E level splitting, and decay times for three Mn^{4+} centers in the GGG crystal at $T = 10$ K.

	Center *A*	Center *B*	Center *C*
Wavelength of excitation peak	660.5 nm	667 nm	670 nm
Wavelength of emission peak	663.5 nm	668 nm	671 nm
Stokes shift	68 cm^{-1}	23 cm^{-1}	22 cm^{-1}
^2E level splitting	80 cm^{-1}	170 cm^{-1}	40 cm^{-1}
Decay time	(1280±90) μs	(445±30) μs	(370±10) μs

C. Decay rate analysis

The temperature dependence of the decay rate of sharp line luminescence associated with the emission of p phonons of energy $\hbar\omega$ is expressed by the formula[6]

$$1/\tau = W_r^0 \coth(\hbar\omega/2kT) + W_n^0\{\exp[-S\langle 2n+1\rangle]\}[S\langle 1+n\rangle]^p/p! , \quad (3)$$

where

$$\langle n\rangle = [\exp(\hbar\omega/kT)-1]^{-1}$$

is the phonon occupation number, S is the Huang-Rhys parameter, k is the Boltzman constant, and W_r^0 and W_n^0 are temperature-independent prefactors of radiative and nonradiative decay rates. The solid line in Fig. 12 represents the best fit of formula (3) to the temperature dependence of the decay rate of center A, treating the parameters describing the electron-phonon coupling as adjustable parameters. The total energy of $p\hbar\omega \approx 15\,070$ cm^{-1}, necessary to cross the gap between the ^2E and the $^4A_2$ states, was kept constant here. The good fit between theory and experiment shown in the figure is obtained using $\hbar\omega = 321$ cm^{-1}, $W_r^0 = 805$ s^{-1}, and $S_0 \approx 0.12$. The results are consistent with those obtained for Mn^{4+} in $Y_3Al_5O_{12}$ (Ref. 4) and $Li_4Ge_5O_{12}$ (Ref. 5) crystals. Additionally, the value of S agrees very well with the Stokes shift $\Delta E = 2S\hbar\omega$ between the PLE and luminescence spectra of center A. A reasonably good fit of Eq. (3) to the temperature dependence of the decay rate of center B can be obtained with similar values of $\hbar\omega$ and S. The energy of the effective phonon $\hbar\omega = 321$ cm^{-1} agrees very well with the energy of the dominating phonon in the Raman spectrum of the GGG:(Mn^{4+};Ca^{2+}) sample (see Fig. 13).

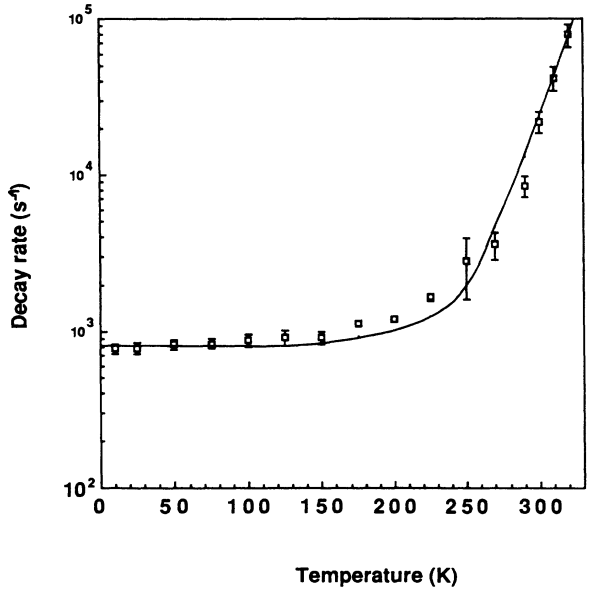

FIG. 12. Temperature dependence of the decay rate of center A. The solid line represents the best fit of Eq. (3) to the experimental data.

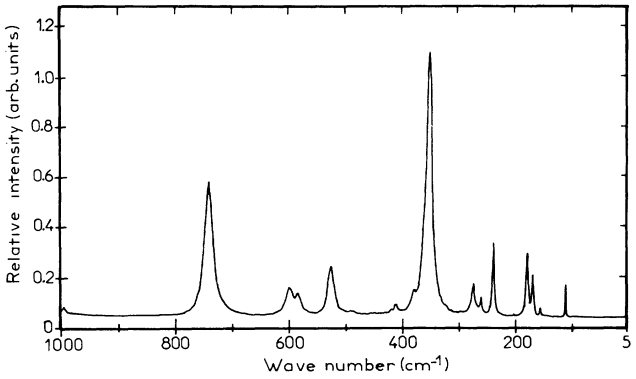

FIG. 13. Room-temperature Raman spectrum of the GGG:(Mn^{4+};Ca^{2+}) sample.

D. The broadening and the Stokes shift of the zero-optical phonon $E_{1/2}(^2E) \rightarrow {}^4A_2$ transition by low-frequency phonons

The large value (about 60 cm^{-1}) of the width of the zero-optical phonon $^2E \rightarrow {}^4A_2$ transition of Mn in the A, B, and C environments cannot be attributed to inhomogeneous broadening. We have checked that the A line emission spectrum is independent of the laser excitation wavelength around 660.5 nm. The excitation spectra of different wavelengths of the A emission line are also the same. Moreover, the A, B, and C decay kinetics are exponential if excited selectively. Lastly, it is difficult to explain the large Stokes shift between the excitation and the emission of a transition in the case of an inhomogeneous broadening. This shift cannot be attributed to a transition to the upper $^2A_{3/2}$ level of the ^2E state (R_2) line), which was carefully checked during the experiment. On the other hand, the long lifetimes of these transitions are inconsistent with very large values of a homogeneous width of 60 cm^{-1}.

To interpret the broadening and the Stokes shift between the excitation and the emission of the $^2E \rightarrow {}^4A_2$ zero-optical phonon transition in the A case at liquid-helium temperature, we propose to use a single-coordinate configuration (SCC) model.[6] The two electronic levels involved in this model are ^2E and $^4A_2$. Each of them is coupled with low-frequency vibrations, the phonon energy $\hbar\omega$ of which is a free parameter (the same for both levels). The energy E_0 of the transition between the true zero-phonon $E_{1/2}$ and zero-phonon $^4A_2$ levels (zero-optical and zero-low-energy phonon) is assumed to be equal to half of the sum of the energies E_{em} and E_{ex} of the peaks of the emission and excitation spectra of the zero-optical phonon transition. These energies are equal to, respectively, $E_0 = 15\,106$ cm^{-1}, $E_{em} = 15\,072$ cm^{-1}, $E_{ex} = 15\,140$ cm^{-1} (the corresponding wavelength of the zero-phonon transition is 662 nm, the excitation and emission peaks being, respectively, at 660.5 and 663.5 nm). The Huang-Rhys S parameter is deduced from the relation $2S\hbar\omega = E_{ex} - E_{em}$. According to the Struck-Fonger theory, the radiative probability of transition be-

tween the initial and final vibronic states, which involves P_u phonons, is proportional to[6]

$$W_{P_u} = e^{-S(2n+1)} \sum_{j=j_0}^{\infty} \frac{(S\langle n\rangle)^j (S\langle 1+n\rangle)^{P_u+j}}{j!(P_u+j)!} , \quad (4)$$

where j is the larger number between 0 and $-P_u$. The stimulated emission cross section and the absorption cross section are deduced from (4) and from McCumber[12] relations taking into account the experimental radiative probability of emission in the 663.5-nm line as equal to 149 s^{-1}. The results are presented in Fig. 14. The fit has been obtained with a phonon of energy $\hbar\omega = 8$ cm^{-1}, and $S = 4.2$.

Such a large value of S explains why we do not observe any zero-phonon line at 15 106 cm^{-1}. The ratio of the zero-phonon line and peak of the band intensities is equal to $\exp(-S)$ (Ref. 6). In this case it is equal to 0.014. It is also a proof that larger-energy phonons, which are responsible for nonradiative transitions, cannot be responsible for the broadening of the $E_{1/2}(^2E) \rightarrow {}^4A_2$ transitions. In such a case the intensity of the zero-phonon line should be much stronger compared to the peak of the spectrum. Therefore, even if zero-phonon transitions are strongly symmetry forbidden, which does not allow one to observe them in one-photon spectra, it should be possible to record them in two-photon excitation since two-photon selection rules allow electric-dipole transitions between ^2E and $^4A_2$ states. The lack of a zero-phonon line in the two-photon spectra provides an additional support for our model.

In general, the *effective* density of phonon states $\rho(\omega)$, which is the density of phonon states weighted by the coupling parameters $|s_k|^2$, is responsible for the linewidth of optical transitions.[13] Although the Raman spectrum of GGG:Mn^{4+} does not reveal any major peaks in the range of 8 cm^{-1}, there is a very weak band which spreads out from 30 cm^{-1}, approximately, to energies very close to that one of the exciting laser line (not shown in Fig. 13). Nevertheless, it is known that Mn^{4+} ions couple with the lattice much stronger than Cr^{3+} (Ref. 4). Carefully measured excitation and emission spectra of GGG:Cr^{3+} show that the Stokes shift (if any) is smaller than 2 cm^{-1} (Ref. 14), although the R linewidth is about 6 cm^{-1} (Ref. 15), which is much more than in the other well-known Cr^{3+}-doped laser materials. Recently, it has been shown that the broadening of Cr^{3+} R lines in GGG is due to magnetic interaction of the dopant with strongly paramagnetic Gd^{3+} ions.[16] Possibly, the large broadening of the R lines and large Stokes shift in the case of GGG:Mn^{4+} also have magnetic origin. In order to obtain more detailed information on electron-lattice coupling in GGG:Mn^{4+}, additional studies would be necessary.

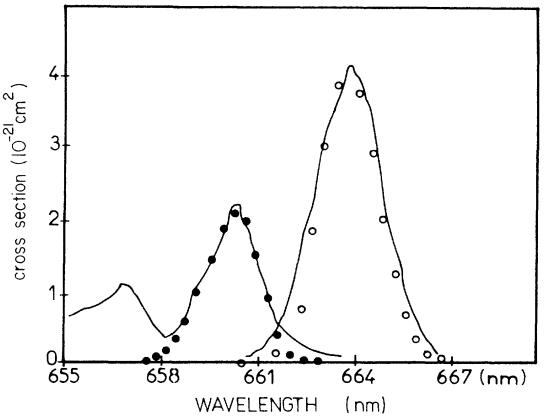

FIG. 14. The stimulated emission and the absorption cross sections for center A at $T = 8$ K. The circles represent the best fit of Struck-Fonger [Eq. (4)] and McCumber theories to the experimental data. ●●●●, absorption cross section; ○○○○, stimulated emission cross section.

V. CONCLUSIONS

The Mn^{4+} spectroscopy in GGG crystals shows features which have not been observed in the other hosts, to the authors' knowledge. The most important one postulated here is the presence of very strong electron-phonon coupling, especially with low-energy phonons, which results in a very large linewidth of optical transitions, which are usually very sharp in other crystals.

Garnets are often considered to be crystals with a large amount of disorder, which leads to large inhomogeneous broadening of optical transitions. Our results show that strong coupling with low-frequency lattice excitations may be responsible for this broadening rather than large disorder. Nevertheless, due to complicated crystallographic structure, a few different sites are occupated by dopants, which was also observed in the case of GGG:Mn^{4+}.

ACKNOWLEDGMENTS

The authors would like to express their thanks to S. Lecocq for crystal orientation and to A. Boukenter and B. Champagnon for measuring the Raman spectra. A. Suchocki is grateful to CNRS and to MENJS for support at University of Lyon I. We are also indebted to DRET and Region Phone-Alpes for financial support of this research.

*Permanent address: Institute of Physics, Polish Academy of Sciences, Al. Lotnikow 32/46, 02-668 Warszawa, Poland.

[1] S. Geschwind, P. Kisliuk, M. P. Klein, J. P. Remeika, and D. L. Wood, Phys. Rev. **126**, 1684 (1962).

[2] B. Henderson and T. P. P. Hall, Proc. Phys. Soc. London **90**, 511 (1967).

[3] L. A. Riseberg and M. J. Weber, Solid State Commun. **9**, 791 (1971).

[4] J. F. Donegan, T. J. Glynn, G. F. Imbusch, and J. P. Remeika, J. Lumin. **36**, 93 (1986).

[5]A. Suchocki, J. D. Allen, and R. C. Powell, Phys. Rev. B **36**, 6729 (1987).

[6]C. W. Struck and W. H. Fonger, J. Chem. Phys. **60**, 1988 (1974); J. Lumin. **10**, 1 (1975).

[7]A. Brenier, C. Pedrini, C. Madej, G. Boulon, and A. Suchocki, J. Phys. (Paris) Colloq. (Suppl. 1) **52**, C7-323 (1991); A. Suchocki, A. Brenier, C. Pedrini, C. Madej, and G. Boulon (unpublished).

[8]T. R. Bader and A. Gold, Phys. Rev. **171**, 997 (1968).

[9]D. Mateika, R. Laurien, and Ch. Rusche, J. Cryst. Growth **56**, 677 (1982).

[10]P. P. Feofilov, *The Physical Basis of Polarized Emission* (Consultants Bureau, New York, 1961).

[11]S. Geller, Z. Kristallogr. **125**, 1 (1967).

[12]D. E. McCumber, Phys. Rev. **134**, A299 (1964).

[13]G. F. Imbusch, W. M. Yen, A. L. Schawlow, D. E. McCumber, and M. D. Sturge, Phys. Rev. **133**, A1029 (1964).

[14]A. Brenier, A. Suchocki, C. Pedrini, G. Boulon (unpublished).

[15]A. Monteil, W. Nie, C. Madej, G. Boulon, Opt. Quantum Electron. **22**, S247 (1990).

[16]A. Monteil, M. Ferreri, and F. Rossi, Phys. Rev. B **43**, 3646 (1991); A. Monteil, J. Phys.: Condens. Matter **2**, 9639 (1990).